

CGC/saturation approach: Impact-parameter dependent model in next-to-leading order and combined HERA data

Michael Sanhueza,^{1,2,*} José Garrido M.,^{3,†} and Miguel Guevara^{1,‡}

¹*Facultad de Ingeniería, Laboratorio DataScience,*

Universidad de Playa Ancha, Leopoldo Carvallo 270, Valparaíso, Chile

²*Centro de Estudios Avanzados, Universidad de Playa Ancha, Traslaviña 450, Viña del Mar, Chile*

³*Departamento de Física, Universidad Técnica Federico Santa María,*

Avda. España 1680, Casilla 110-V, Valparaíso, Chile

In this paper we confront the next-to-leading order (NLO) CGC/saturation approach of Ref. [1] with the experimental combined HERA data and obtain its parameters. The model includes two features that are in accordance with our theoretical knowledge of deep inelastic scattering. These consist of: *i*) the use of analytical solution for the non-linear Balitsky-Kovchegov (BK) evolution equation and *ii*) the exponential behavior of the saturation momentum on the impact parameter b -dependence, characterized by $Q_s \propto \exp(-mb)$ which reproduce the correct behaviour of the scattering amplitude at large b in accord with Froissart theorem. The model results are then compared to data at small- x for the structure function of the proton F_2 , the longitudinal structure function F_L , the charm structure function $F_2^{c\bar{c}}$, the exclusive vector meson ($J/\psi, \phi, \rho$) production and Deeply Virtual Compton Scattering (DVCS). We obtain a good agreement for the processes in a wide kinematic range of Q^2 at small x . Our results provide a strong guide for finding an approach, based on Color Glass Condensate/saturation effective theory for high energy QCD, to make reliable predictions from first principles as well as for forthcoming experiments like the Electron-Ion Collider and the LHeC.

PACS numbers: 12.38.Cy, 12.38g, 24.85.+p, 25.30.Hm

Contents

I. Introduction	1
II. Description of inclusive and exclusive diffractive processes	3
A. Inclusive processes: Total DIS cross-section and proton structure functions	3
B. Exclusive diffractive processes: Deeply virtual Compton scattering and exclusive vector meson production	3
III. CGC/saturation NLO dipole model	5
A. $q\bar{q}$ dipole-proton scattering amplitude	5
B. Phenomenological input: Impact parameter dependence of the saturation scale	6
IV. Numerical results and discussion	7
V. Conclusions	14
VI. Acknowledgements	16
References	16

I. INTRODUCTION

The goal of this paper is to confront the next-to-leading order (NLO) Color Glass Condensate (CGC)/saturation approach of Ref. [1] with the experimental combined HERA data and obtain its parameters via fit. In order to contrast with experimental data, it was select deep inelastic processes using the CGC/saturation equations from Ref.[2] in a simple version of the non-linear Balitsky-Kovchegov (BK) equation [3]. The authors of Ref. [1] proposed the way to take into account the NLO corrections, which coincides with other attempts on the market, as far as the linear dynamics is concerned, but introduce the non-linear evolution which guarantees the correct high energy asymptotic behaviour of the scattering amplitude. They include the re-summation procedure suggested in Refs. [4–6], to fix the BFKL kernel in the NLO. Specifically, the rapidity variable was introduced in the same way as in Ref. [7].

Nevertheless, a different way to account the non-linear corrections was suggested which leads to additional change of the NLO kernel of the evolution equation. The advantage of the BFKL kernel [8, 9], is that it leads to the scattering amplitude satisfying high-energy limits, which follows from the approach of Ref. [10] (see Refs. [11, 12]) concerning to the NLO-BK [3] evolution equation [13–19].

It is widely accepted that finding the correct NLO approximation for the nonlinear evolution is one of the most important and urgent problem in the theoretical understanding of high energy scattering, since the BFKL Pomeron intercept is too large leaving the theoretical estimates in severe qualitative contradiction with experimental data. In fact, the two essential parameters that determine the high energy scattering are the BFKL Pomeron [8] intercept, which is equal to $2.8\bar{\alpha}_S$, and leads to the energy behaviour of the scattering amplitude $N \propto \exp(2.8\bar{\alpha}_S \ln(\frac{1}{x}))$ and the energy behavior of the saturation momentum $Q_s^2 \propto \exp(4.88\bar{\alpha}_S \ln(\frac{1}{x}))$. Both scenarios show the increase in the leading order CGC approach, which is inconsistent with the existing experimental data. Hence, the large NLO corrections remain the singular path forward, now as well as two decades ago. In Ref. [1] it was found the analytical solution of the nonlinear BK equation taking into account the main features of the NLO corrections to the BFKL kernel such is able to describe the experimental HERA data.

The model which is based on CGC/saturation effective theory for high energy QCD (see Ref. [20] for a review), include the impact parameter dependence of the scattering amplitude. Within this framework, the scattering amplitude falls down at large impact parameters b as a power of b . Such a power-like decrease leads to the violation of the Froissart theorem [21]. Therefore, we have no choice but to build a model because CGC/saturation equations cannot reproduce the correct behavior of the scattering amplitude at large impact parameters [22, 23]. In accordance with the geometric scaling behavior of the scattering amplitude [24, 25] and guided by the semi-classical solution to the CGC/saturation equations [26], we incorporate the non-perturbative impact parameter behavior into the saturation momentum. In most cases, the models include the non-perturbative b -behavior of the scattering amplitude and has been used widely in all, so called saturation models [11, 27–47].

In the choice of the nonperturbative behavior of the saturation scale, instead to use the common approach proportional to $\exp(-b^2/B)$ which disagrees the theoretical knowledge of QCD at high energies [10, 21], we will parametrize as follows [11, 46, 47]:

$$Q_s^2(b, Y) \propto (S(b, m))^{\frac{1}{\bar{\gamma}}} \quad (1)$$

where $S(b)$ is the Fourier image of $S(Q_T) = 1/\left(1 + \frac{Q_T^2}{m^2}\right)^2$ and the value of $\bar{\gamma}$ we will discuss in section III. In the vicinity of the saturation scale, this b dependency leads to a significant b -dependence of the scattering amplitude, which is proportional to $\exp(-mb)$ for $b \gg 1/m$, consistent with the Froissart theorem [21]. We want to stress the fact that the model's b -dependence is congruent with perturbative QCD calculations for large values of momentum transferred (Q_T), leading to a power-like behavior in the scattering amplitude at high Q_T .

With these observations and remarks, in this paper we will examine how the CGC/saturation NLO model reproduces the combined HERA data and carry out a detailed analysis of this data. Furthermore, due to the simplicity of the theoretical understanding of the deep inelastic structure function F_2 and the reduced cross-section σ_r , these processes have been measured with high accuracy by H1 and ZEUS collaboration [48, 49] containing extremely small error bars which implies that describing this data is a challenge for any theoretical approach. Fitting to this observable allow us to extract all phenomenological parameters that are introduced in the model. After determining the values of all phenomenological parameters we calculate and compared the theoretical results to data at small- x for the structure function of the proton F_2 , the longitudinal structure function F_L , the charm structure function $F_2^{c\bar{c}}$, the exclusive vector meson ($J/\psi, \phi, \rho$) production and Deeply Virtual Compton Scattering (DVCS).

Our results provide a strong guide in the continuous process for finding an approach, based on Color Glass Condensate/saturation effective theory for high energy QCD, to make reliable predictions from first principles, as well as for forthcoming experiments like the Electron-Ion Collider [50] and the LHeC [51]. Another important application is to use the dipole amplitude for the production of dijets in p-p and p-Pb collisions [52] or the structure of the soft Pomeron in CGC [53]. This paper is organized as follows. In section II, we present a brief overview of the framework for computing the total DIS cross-section, structure functions, and exclusive diffractive processes within the color dipole approach. In section III, we specify our approach of the CGC/saturation NLO dipole model introducing the main formulation which we use for describing the experimental data. In particular, we introduce the phenomenological parameters, which must to be calculated in the nonperturbative QCD approach. In section IV we discuss the numerical results. We summarize our results in the conclusion.

II. DESCRIPTION OF INCLUSIVE AND EXCLUSIVE DIFFRACTIVE PROCESSES

A. Inclusive processes: Total DIS cross-section and proton structure functions

The observables in deep inelastic scattering (DIS) can be expressed through the following scattering amplitudes (see Ref. [20] and references therein):

$$N_{L,T}(Q, Y; b) = \int \frac{d^2r}{4\pi} \int_0^1 dz |\Psi_{L,T}^{\gamma^*}(Q, r, z)|^2 N(r, Y; b) \quad (2)$$

where $Y = \ln(1/x_{Bj})$ and x_{Bj} is the Bjorken x . z is the fraction of the light cone momentum of the virtual photon carried by quark. Q is the photon virtuality and L, T denote the longitudinal and transverse polarizations of the virtual photon. In the dipole picture of DIS at high energies, the interactions are characterized by the features shown in Eq. (2). The process occurs as follows: in the first stage the virtual photon decay into quark-antiquark pair, described by $|\Psi_{L,T}^{\gamma^*}(Q, r, z)|^2$. During the second stage, the color dipole proceeds to interact with the target (proton) represented by $N(r, Y; b)$, which is the imaginary part of the forward $q\bar{q}$ dipole-proton scattering amplitude with transverse dipole size r and impact parameter b .

The wave function for $|\Psi_{L,T}^{\gamma^*}(Q, r, z)|^2 \equiv (\Psi^* \Psi)_{L,T}^{\gamma^*}$ is well known (see Ref. [20] and references therein).

$$(\Psi^* \Psi)_T^{\gamma^*} = \frac{2N_c}{\pi} \alpha_{\text{e.m.}} \sum_f e_f^2 \{ [z^2 + (1-z)^2] \epsilon_f^2 K_1^2(\epsilon_f r) + m_f^2 K_0^2(\epsilon_f r) \}, \quad (3)$$

$$(\Psi^* \Psi)_L^{\gamma^*} = \frac{8N_c}{\pi} \alpha_{\text{e.m.}} \sum_f e_f^2 Q^2 z^2 (1-z)^2 K_0^2(\epsilon_f r), \quad (4)$$

with

$$\epsilon_f^2 = m_f^2 + z(1-z)Q^2 \quad (5)$$

where $\alpha_{\text{e.m.}}$ is the electromagnetic fine structure constant, N_c denotes the number of colors and e_f is the electric charge of a quark with flavor f and mass m_f . In $c\bar{c}$ scattering, the mass of the charm quark (about $m_c = 1.4 \text{ GeV}$) is not small and we took this into account by replacing x as $x_c = x_{Bj}(1 + 4m_c^2/Q^2)$. Using Eq. (2), Eq. (3) and Eq. (4) we can write the main observables in DIS as follows:

$$\sigma_{T,L}^{\gamma^* p}(Q^2, x) = 2 \int d^2b N_{T,L}(Q, Y; b); \quad (6a)$$

$$F_2(Q^2, x) = \frac{Q^2}{4\pi^2 \alpha_{\text{e.m.}}} [\sigma_T^{\gamma^* p}(Q^2, x) + \sigma_L^{\gamma^* p}(Q^2, x)]; \quad (6b)$$

$$F_2^{c\bar{c}}(Q^2, x) = \frac{Q^2}{4\pi^2 \alpha_{\text{e.m.}}} [\sigma_T^{c\bar{c}, \gamma^* p}(Q^2, x) + \sigma_L^{c\bar{c}, \gamma^* p}(Q^2, x)]; \quad (6c)$$

$$F_L(Q^2, x) = \frac{Q^2}{4\pi^2 \alpha_{\text{e.m.}}} \sigma_L^{\gamma^* p}(Q^2, x); \quad (6d)$$

The reduced cross-section σ_r is expressed in terms of the inclusive proton structure functions F_2 and F_L as

$$\sigma_r(Q^2, x, y) = F_2(Q^2, x) - \frac{y^2}{1 + (1-y)^2} F_L(Q^2, x) \quad (7)$$

where $y = Q^2/(sx)$ denotes the inelasticity variable and \sqrt{s} indicates the center of mass energy in ep collisions.

B. Exclusive diffractive processes: Deeply virtual Compton scattering and exclusive vector meson production

In the dipole approach, the scattering amplitude for the exclusive diffractive processes $\gamma^* + p \rightarrow E + p$, with the final state a real photon $E = \gamma$ in DVCS or vector meson $E = J/\psi, \phi, \rho$ can be written in terms of a convolution of

the dipole amplitude N and the overlap wave functions of the photon and the exclusive final-state particle. The main formula for exclusive diffractive processes take the form [34]:

$$\mathcal{A}_{T,L}^{\gamma^* p \rightarrow Ep}(x, Q, \Delta) = i \int d^2 \mathbf{r} \int_0^1 \frac{dz}{4\pi} \int d^2 \mathbf{b} (\Psi_E^* \Psi)_{T,L} e^{-i[\mathbf{b} - (1-z)\mathbf{r}] \cdot \Delta} N(r, Y; b) \quad (8)$$

where $|\Delta|^2 = -t$, and t represents the squared momentum transfer. The phase factor $\exp(i(1-z)\mathbf{r} \cdot \Delta)$ is due to the non-forward wave-functions contribution [54].

In terms of the scattering amplitude of Eq. (8), the differential cross-section for exclusive diffractive processes may be written as [31, 34]

$$\frac{d\sigma_{T,L}^{\gamma^* p \rightarrow Ep}}{dt} = \frac{1}{16\pi} \left| \mathcal{A}_{T,L}^{\gamma^* p \rightarrow Ep} \right|^2 (1 + \rho^2) R_g^2 \quad (9)$$

where

$$\sigma_{T,L}^{\gamma^* p \rightarrow Ep} = \int dt \frac{d\sigma_{T,L}^{\gamma^* p \rightarrow Ep}}{dt} \quad (10)$$

and

$$B_D = \ln \left(\frac{d\sigma_{T,L}^{\gamma^* p \rightarrow Ep}}{dt} / \frac{d\sigma_{T,L}^{\gamma^* p \rightarrow Ep}}{dt} \Big|_{t=0} \right) \quad (11)$$

are the two main observables that we are going to use to calculate our theoretical estimates. In order to account the missing real part of Eq. (8), a multiplicative factor $(1 + \rho^2)$ must be added, where ρ is the ratio of the real to imaginary parts of the scattering amplitude which show Regge-type behavior at high energies [55–57]

$$\rho = \tan(\pi\beta/2), \quad \text{with } \beta \equiv \frac{\partial \ln(\mathcal{A}_{T,L}^{\gamma^* p \rightarrow Ep})}{\partial \ln(1/x)} \quad (12)$$

where the multiplicative factor R_g take into account the skewedness effect and is defined by [58]

$$R_g = \frac{2^{2\beta+3} \Gamma(\beta + 5/2)}{\sqrt{\pi} \Gamma(\beta + 4)} \quad (13)$$

For deeply virtual Compton scattering (DVCS) the overlap wave function only has transversal contribution. Similar to Eq. (3) where a sum over quark flavors should be done, the equation read as

$$(\Psi_\gamma^* \Psi)_T^{(DVCS)} = \frac{2N_c}{\pi} \alpha_{\text{em}} \sum_f e_f^2 \{ [z^2 + (1-z)^2] \epsilon_f K_1(\epsilon_f r) m_f K_1(m_f r) + m_f^2 K_0(\epsilon_f r) K_0(m_f r) \} \quad (14)$$

For vector meson diffractive production, we have wave functions exclusively for mesons composed of heavy quarks. The J/ψ is the most commonly cited example. Nevertheless, it is important to take into account that the charm quark's mass is not very large, and corrections can be crucial. For all other mesons, confinement corrections are substantial, and the wave function, motivated by heavy quark mesons, can only be considered as pure phenomenological assumptions. The overlap integrals are represented according to the prescription from Ref. [34]

$$(\Psi_V^* \Psi)_T = \hat{e}_f e \frac{N_c}{\pi z(1-z)} \{ m_f^2 K_0(\epsilon_f r) \phi_T(r, z) - [z^2 + (1-z)^2] \epsilon_f K_1(\epsilon_f r) \partial_r \phi_T(r, z) \} \quad (15)$$

$$(\Psi_V^* \Psi)_L = \hat{e}_f e \frac{N_c}{\pi} 2Qz(1-z) K_0(\epsilon_f r) \left[M_V \phi_L(r, z) + \frac{m_f^2 - \nabla_r^2}{M_V z(1-z)} \phi_L(r, z) \right] \quad (16)$$

$$\phi_{T,L}(r, z) = \mathcal{N}_{T,L} z(1-z) \exp \left(-\frac{m_f^2 \mathcal{R}^2}{8z(1-z)} - \frac{2z(1-z)r^2}{\mathcal{R}^2} + \frac{m_f^2 \mathcal{R}^2}{2} \right) \quad (17)$$

where $\nabla_r^2 \equiv (1/r)\partial_r + \partial_r^2$, M_V is the meson mass and the effective charge \hat{e}_f takes the values of $2/3$, $1/3$, or $1/\sqrt{2}$ for J/ψ , ϕ , or ρ mesons respectively. $m_f = 140$ MeV is the mass used in the above equations. The parameters $\mathcal{N}_{T,L}$ and \mathcal{R} are from Table 2 in Ref. [34].

III. CGC/SATURATION NLO DIPOLE MODEL

A. $q\bar{q}$ dipole-proton scattering amplitude

In order to calculate the total cross-section, the proton structure functions in DIS, exclusive diffractive vector meson production and DVCS we need to use the $q\bar{q}$ dipole-proton forward scattering amplitude. In Ref. [1] the analytical solution for the nonlinear BK equation was found at NLO BFKL kernel in the saturation domain. The authors proposed the way to take into account the NLO corrections introducing the non-linear evolution which guarantees the correct high energy asymptotic behaviour of the scattering amplitude. They include the re-summation procedure suggested in Refs. [4–6], to fix the BFKL kernel in the NLO. Specifically, the rapidity variable was introduced in the same way as in Ref. [7]. Nevertheless, a different way to account the non-linear corrections was suggested: the anomalous dimension was derived in the region of large $\tau = r^2 Q_s^2$ in the limit when $\gamma \rightarrow 0$ by using the kernel in γ -representation for the leading twist in place of the full BFKL kernel (see equation 90 from Ref. [1]), which corresponds to the sum of two types of logarithms [10]. The advantage of the BFKL kernel [8, 9], is that it leads to the scattering amplitude satisfying high-energy limits, which follows from the approach of Ref. [10] (see Refs. [11, 12]) concerning to the NLO-BK [3] evolution equation [13–19].

In the CGC/saturation NLO dipole model, the color $q\bar{q}$ dipole-proton scattering amplitude is given by [1, 47]:

$$N(z) = \begin{cases} N_0 e^{z\bar{\gamma}} & \text{for } z \leq 1; \\ a \left(1 - e^{-\Omega(z)}\right) + (1 - a) \frac{\Omega(z)}{1 + \Omega(z)} & \text{for } z > 1; \end{cases} \quad (18)$$

where $a = 0.65$ describes the exact solution of nonlinear BK equation within accuracy less than 2.5 % [47, 59] and the function $\Omega(z)$ has the following form [1, 47]

$$\Omega = \Omega_0 \left\{ \cosh(\sqrt{\sigma}z) + \frac{\bar{\gamma}}{\sqrt{\sigma}} \sinh(\sqrt{\sigma}z) \right\}, \quad \text{with } \sigma = \frac{\bar{\alpha}_S}{\lambda(\bar{\alpha}_S)(1 + \bar{\alpha}_S)}; \quad (19)$$

and Ω_0 has the same numerical value as N_0 , ensuring the proper behavior of the solution for Eq. (18). N_0 is the value of the scattering amplitude at $\tau = 1$. In principle, the value of N_0 can be calculated using the linear evolution equation with the initial conditions. However, it depends on the phenomenological parameters of this initial condition. As a result, we adopt N_0 as a parameter to be found through fitting. The variable z is defined as

$$z = \xi_s + \xi, \quad \text{with } \xi_s = \ln(Q_s^2(Y, b)/Q_s^2(Y = 0, \mathbf{b})), \quad \xi = \ln(r^2 Q_s^2(Y = 0, \mathbf{b})); \quad (20)$$

The use of this variable indicates the main idea of the approach in the region for $\tau = r^2 Q_s^2 > 1$. The goal is to establish a correspondence between the solution of the nonlinear equation and the solution of the linear equation in the kinematic region described by $N = N_0 e^{z\bar{\gamma}}$.

The critical anomalous dimension and the energy behavior of the saturation scale was determined in NLO in Ref. [1] which has the following form:

$$\bar{\gamma} = \bar{\gamma}_\eta(1 + \lambda_\eta), \quad \text{with } \bar{\gamma}_\eta = \sqrt{2 + \bar{\alpha}_S} - 1; \quad (21)$$

and

$$\lambda = \frac{\lambda_\eta}{1 + \lambda_\eta}, \quad \text{with } \lambda_\eta = \frac{1}{2} \frac{\bar{\alpha}_S}{(3 + \bar{\alpha}_S - 2\sqrt{2 + \bar{\alpha}_S})}; \quad (22)$$

where $\eta = Y - \xi$ is a new energy variable and $Y = \ln(1/x)$ is the rapidity of the dipole.

We use a different way to introduce the parameters from the experimental data: expanding the linear solution of Eq. (18) to the region $\tau < 1$, replacing $\bar{\gamma}$ by the following expression:

$$\bar{\gamma} \rightarrow \bar{\gamma} + \frac{\ln(1/\tau)}{2\kappa\lambda Y}, \quad \text{with } \kappa = \frac{\chi''(\bar{\gamma})}{\chi'(\bar{\gamma})} = \frac{\frac{d^2\omega(\bar{\gamma}_\eta)}{d\bar{\gamma}_\eta^2}}{\frac{d\omega(\bar{\gamma}_\eta)}{d\bar{\gamma}_\eta}} \quad (23)$$

this equation was derived in Ref. [60] and the results from saturation models [11, 27–47] demonstrate a strong agreement with the experimental data for $x \leq 0.1$.

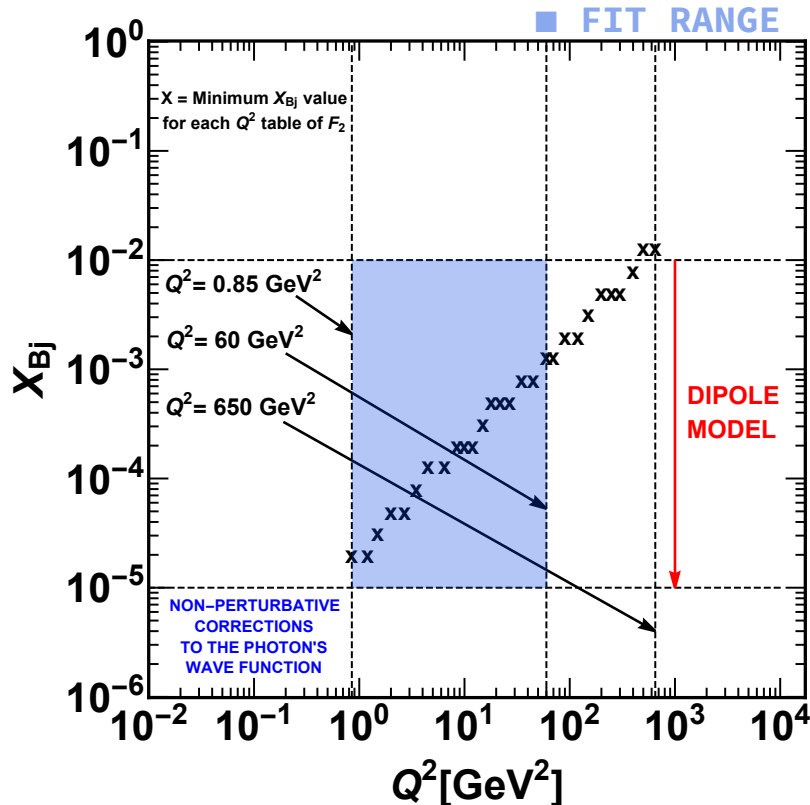


FIG. 1: Fit range in the kinematic plane Q^2 - x_{Bj} . The picture displays the non-perturbative region of the photon's wave function $Q^2 < 0.85 \text{ GeV}^2$ and the region in which the dipole model is valid for $x < 10^{-2}$. The marker represents the minimum x value found in the experimental data of F_2 within each Q^2 table from H1 and ZEUS collaborations [48] in the considered kinematic region.

B. Phenomenological input: Impact parameter dependence of the saturation scale

Until now, we have only incorporated one phenomenological parameter: N_0 which determines the scattering amplitude at $r^2 Q_s^2 = 1$. However, we must define the initial conditions at $Y = 0$ for the linear evolution equation in the region where $\tau = r^2 Q_s^2 \leq 1$. This involves the value of saturation scale at $b = 0$ and how it changes with the impact parameter b . Nevertheless, both aspects is constrained to the non-perturbative realm of QCD, and the current understanding is limited, leading to the suggestion of a phenomenological parameterization. We use the following expression to represent the saturation momentum [11, 46]:

$$Q_s^2(Y, b) = Q_s^2(Y = 0, b = 0) S(b)^{1/\bar{\gamma}} e^{\lambda Y} = Q_0^2 (m b K_1(m b))^{1/\bar{\gamma}} e^{\lambda Y}; \quad (24)$$

The values of Q_0^2 and m will be fixed by a fit to the F_2 and the reduced cross-section. Previous results of fitting gives the value of $Q_0^2 = 0.15 - 0.25 \text{ GeV}^2$. We expect $m \approx 0.4 \div 0.85$ since $m = 0.72 \text{ GeV}$ is the scale for the electromagnetic form factor of the proton, while $m \approx 0.5 \text{ GeV}$ is the scale for so called gluon mass [11]. λ and $\bar{\gamma}$ are defined using the respective expressions provided in Eq. (21), Eq. (22) and Eq. (23). However, we consider $\bar{\alpha}_S$ as the fourth parameter of our model, which we expect $\bar{\alpha}_S \approx 0.10$ according to the predictions in the calculations for NLO (see figure 1 in Ref. [47]) obtaining a value for $\lambda = 0.2$, which is the typical value that is necessary to describe DIS data [45]. It is worthwhile mentioning that the NLO corrections to the energy dependence of the saturation momentum gives considerable contributions at small values of $\bar{\alpha}_S$.

In summary, we include three phenomenological parameters originating from the initial conditions, and their values are obtained through the fitting procedure with experimental data.

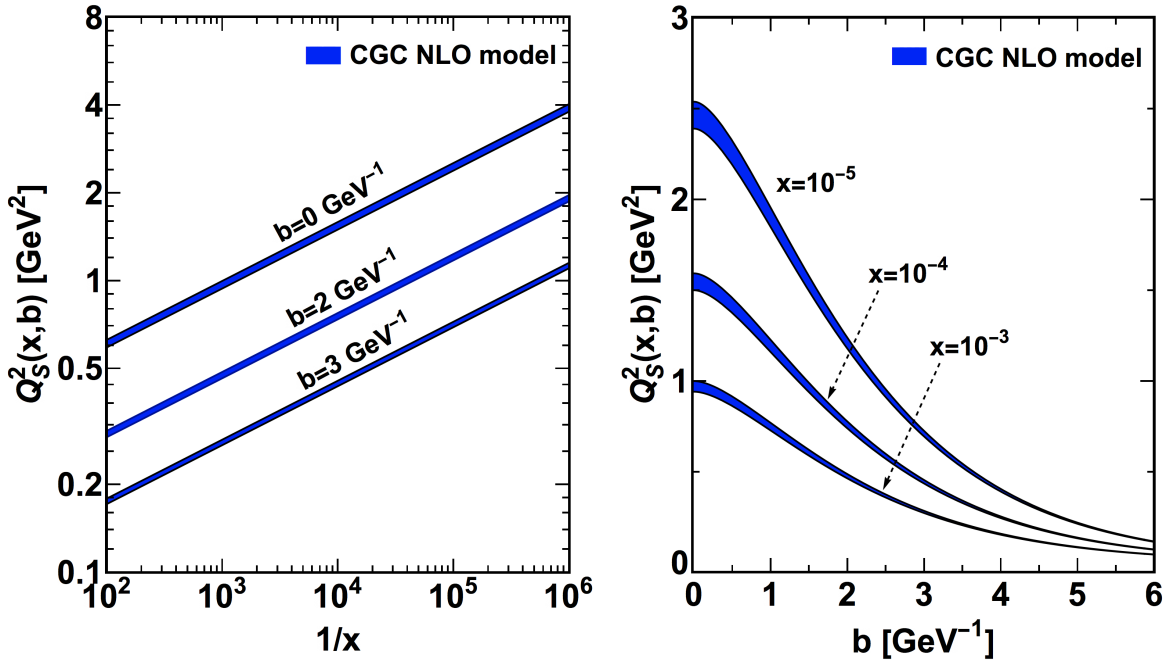


FIG. 2: Left: The saturation scale extracted from the CGC/saturation NLO dipole model with parameters from table I as a function of $1/x$ for different values of b . Right: The saturation scale as a function of impact parameter b for different fixed values of x . In both graphs, the lower and upper lines within the band represent the results using the parameter values specified in Table I, where the charm mass is set to $m_c = 1.40, 1.27$ GeV, respectively.

IV. NUMERICAL RESULTS AND DISCUSSION

Set	Dipole amplitude				Wave function		Minimization	
	$\bar{\alpha}_S$	N_0	Q_0^2 (GeV ²)	m (GeV)	$m_{u,d,s}$ (MeV)	m_c (GeV)	$\chi^2/\text{d.o.f.}$	Q^2/GeV^2
I	0.1027	0.1029	0.8278	0.4212	140	1.4	360.7/346 = 1.042	[0.85, 60]
II	0.1027	0.0927	0.9235	0.4254	140	1.27	433.4/346 = 1.252	[0.85, 60]

TABLE I: Parameters of the CGC/saturation NLO dipole model: $\bar{\alpha}_S$, N_0 , Q_0^2 and m determined from fits to F_2 and reduced cross-section σ_r from the combined H1 and ZEUS data [48] in the range $0.85 \text{ GeV}^2 < Q^2 < 60 \text{ GeV}^2$ and $x \leq 10^{-2}$. Results are shown for fixed light quark masses and two fixed values of the charm quark masses (see the text for details).

As we have addressed previously, 4 free parameters are present in the model, and they are derived from the fit. Within our fit, we consider data points for both the reduced cross-section σ_r and deep inelastic structure function F_2 from H1 and ZEUS collaborations [48]. The data are chosen from the kinematic region $0.85 \text{ GeV}^2 < Q^2 < 60 \text{ GeV}^2$ and $x \leq 10^{-2}$. The lower Q^2 limit arises due to non-perturbative corrections applied to the virtual photon's wave function, while the upper limit is established based on two criteria: $x \leq 10^{-2}$ and contribution of the additional term in $\bar{\gamma}$ outlined in Eq. (23) is small. Our choice to employ the maximum x value is based by the need to guarantee low x values, considering that the BK equation is applicable exclusively at small- x , an essential condition for the valid application of our theoretical equations, as well as the practical goal of including as much data as possible in the fitting process. In Fig. 1 the fitting range within the kinematic plane of Q^2 - x_{Bj} is depicted. The illustration delineates the non-perturbative sector of the photon's wave function ($Q^2 < 0.85 \text{ GeV}^2$) as well as the range where the dipole model is applicable ($x < 10^{-2}$). The symbol “X” represents the smallest x value found in the experimental data of F_2 within each Q^2 table from the H1 and ZEUS collaborations [48] in the specified kinematic region. The vertical lines show the ranges of our fit $Q^2 \in [0.85, 60] \text{ GeV}^2$ as well as the range where the F_2 was predicted outside the range fit for $Q^2 < 650 \text{ GeV}^2$. In the χ^2 calculation, the statistical and systematic experimental uncertainties were added in quadrature. With the extracted parameters, we subsequently confront the model results for F_2 , F_L , and F_2^{cc} with the

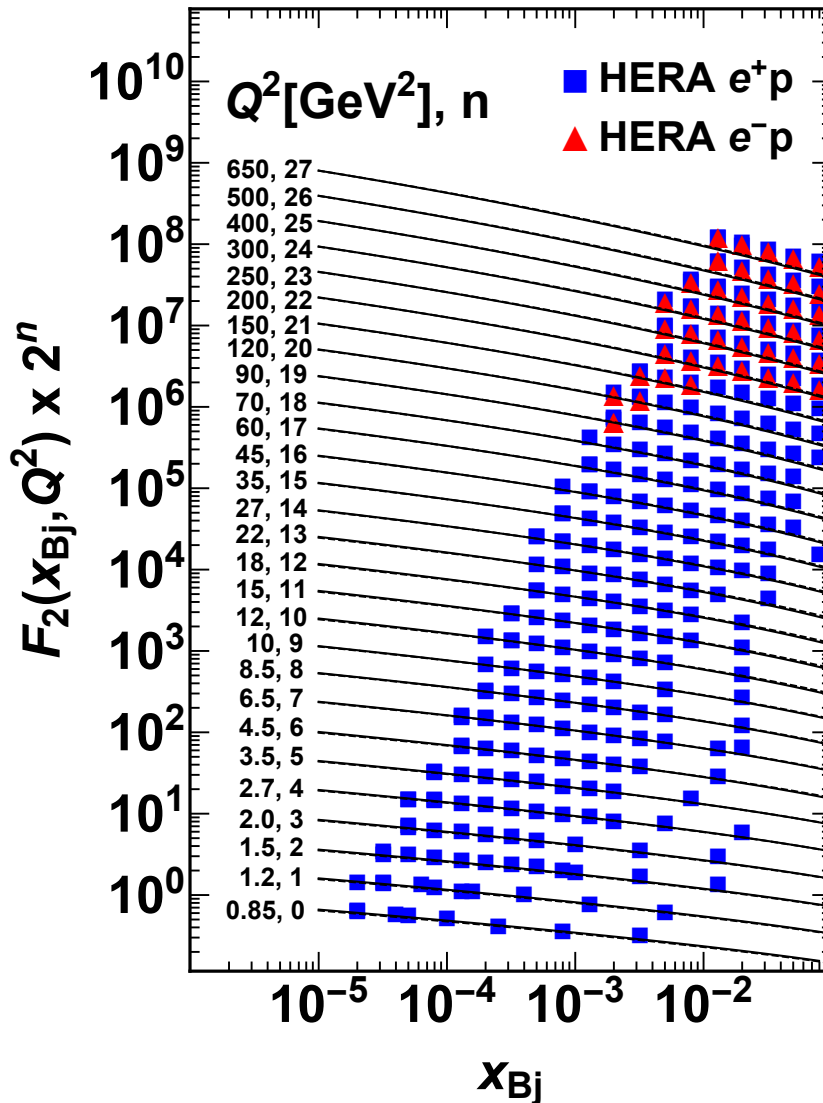


FIG. 3: Results for the structure function $F_2(x, Q^2)$ as a function of x , for different values of Q^2 . The solid and dashed lines are obtained using two distinct sets of parameters from table I corresponding to charm mass values of $m_c = 1.4, 1.27$ GeV, respectively. The theoretical estimates as well as the experimental data are multiplied by factor 2^n and the values of n are specified in the plot. The experimental data are from H1 and ZEUS collaborations [48].

HERA data covering both the kinematic region as defined earlier and regions outside it, which include small values of $Q^2 \leq 0.85$ GeV² and large values of $Q^2 \geq 60$ GeV².

The values of parameters derived from our fits are presented in Table I. We want to emphasize that quark masses were not subjected to fitting. Instead, we have considered the masses of light quarks ($m_u = m_d = m_s$) as $m_u = 140$ MeV, which we consider the standard infra-red cutoff in our approach. Furthermore, two sets have been selected: Set I which contain the parameters using the saturation momentum of Eq. (24) including the mass of the charm quark fixed at $m_c = 1.4$ GeV and Set II where the mass of the charm quark is fixed at $m_c = 1.27$ GeV.

At the saturation scale, the forward $q\bar{q}$ dipole scattering amplitude N undergoes a rapid increase as x decreases, and the amplitude N becomes significant, when non-linear gluon recombination effects turns into as prominent as gluon radiation. What differentiates the NLO dipole model from others is to employ Eq. (24) instead of $Q_s(x, b) \propto \exp(-b^2/B)$ that was used in other saturation models [33–37, 40, 45], which Eq. (24) provide the correct large b

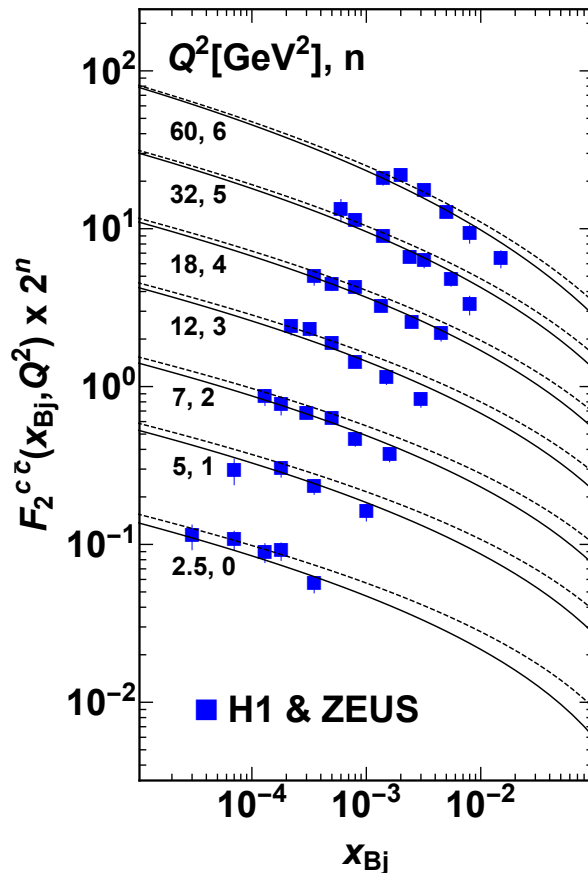


FIG. 4: Results for charm structure function $F_2^{c\bar{c}}(x, Q^2)$ as a function of x , for different values of Q^2 . We used the parameter set I with solid lines ($m_c = 1.4 \text{ GeV}$) and parameter set II with dashed lines ($m_c = 1.27 \text{ GeV}$). The theoretical estimates as well as the experimental data are multiplied by factor 2^n and the values of n are specified in the plot. The experimental data are from H1 and ZEUS collaboration [49], assuming $\sigma_r^{c\bar{c}} \approx F_2^{c\bar{c}}$ (see the text for explanation).

behavior for the scattering amplitude in accord with Froissart theorem [21]. This difference causes the scattering amplitude to increase rapidly in this parametrization, influencing the high-energy predictions significantly. Following Refs. [31, 34, 44, 45], we define the saturation scale $Q_S^2 = 1/r_S^2$, where r_S is the saturation radius, as a scale where the dipole scattering amplitude has a value $N(x, r_S, b) = (1 - \exp(-1/2)) = 0.4$. It is worth mentioning that the saturation scale Q_S^2 differs from our phenomenological parametrization of Eq. (24) with different lower subscript s . In Fig. 2 (left panel), we plot the saturation scale extracted from CGC/saturation NLO dipole model as a function of $1/x$ at different impact parameters b . Certainly, one can observe that the saturation scale, when represented as a function of $1/x$, exhibits a faster growth for collisions with smaller impact parameters, such as those close to central collisions ($b \approx 0$). Additionally, the saturation scale may exhibit substantial variations at distinct impact parameters. This intricate pattern underscores the importance of considering the impact parameter dependence of the saturation scale. In Fig. 2 (right panel) we show the saturation scale as a function of impact parameter b for different fixed values of x . In Fig. 2, the shaded region illustrates the theoretical uncertainties associated with our freedom to select different charm quark mass values within $1.27 \div 1.4 \text{ GeV}$. We notice that within the x range, our saturation scale is in agreement with the existing HERA data.

We only can contrast the model with Refs. [11, 46, 47] since in all other saturation models the assumptions of the saturation scale were made based on Gaussian behavior which contradict the theoretical information. In Ref. [11], the $\bar{\alpha}_S$ value is within the range $\bar{\alpha}_S \approx 0.14 - 0.15$, whereas in Ref. [47] $\bar{\alpha}_S$ falls in the range $\bar{\alpha}_S \approx 0.09 - 0.04$, and in this paper we have found $\bar{\alpha}_S \approx 0.10$. As we have discussed previously we have obtained $\lambda \approx 0.20$, and this parameter is essential for determining the energy dependence of the saturation scale which is necessary to describe HERA data.

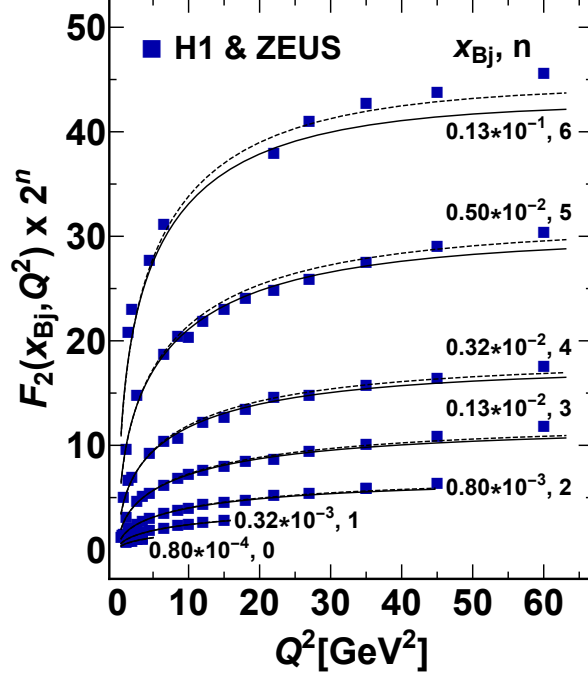


FIG. 5: Results for deep inelastic structure function $F_2(x, Q^2)$ as a function of Q^2 at fixed values of x . The theoretical estimates as well as the experimental data are multiplied by factor 2^n and the values of x and n are specified in the plot. We use the parameters set given in table I with $m_c = 1.4 \text{ GeV}$ in solid lines and $m_c = 1.27 \text{ GeV}$ in dashed lines. The experimental data are from H1 and ZEUS collaborations [48].

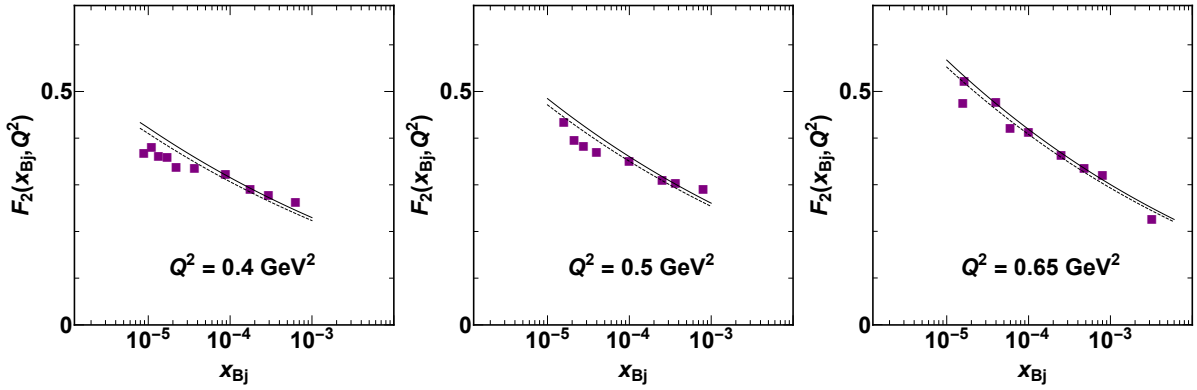


FIG. 6: Results for the structure function $F_2(x, Q^2)$ as a function of x at low values of $Q^2 < 0.85 \text{ GeV}^2$. The solid lines correspond to parameters of set I ($m_c = 1.4 \text{ GeV}$) and the dashed lines correspond to parameters of set II ($m_c = 1.27 \text{ GeV}$). The experimental data are from H1 and ZEUS collaboration [48].

The value of Q_0^2 found via χ^2 is smaller than in Ref. [11] and Ref. [47]. The value of m is smaller than the typical mass in the electromagnetic form factor of the proton, but it is within the range we had expected.

With the parameters presented in table I, extracted from the χ^2 fit to F_2 and reduced inclusive DIS cross-section σ_r , we now proceed to compute the structure function of the proton F_2 , the longitudinal structure function F_L and the charm structure function $F_2^{c\bar{c}}$ (employing Eqs. (6b),(6c),(6d) and (18)) and confront to the combined HERA data sets. The quality of the fit one can see from Fig. 3. Additionally, we expand our theoretical estimates to high Q^2 values and the agreement with data is quite good. We want to emphasize that in this particular kinematic region ($Q^2 > 60 \text{ GeV}^2$)

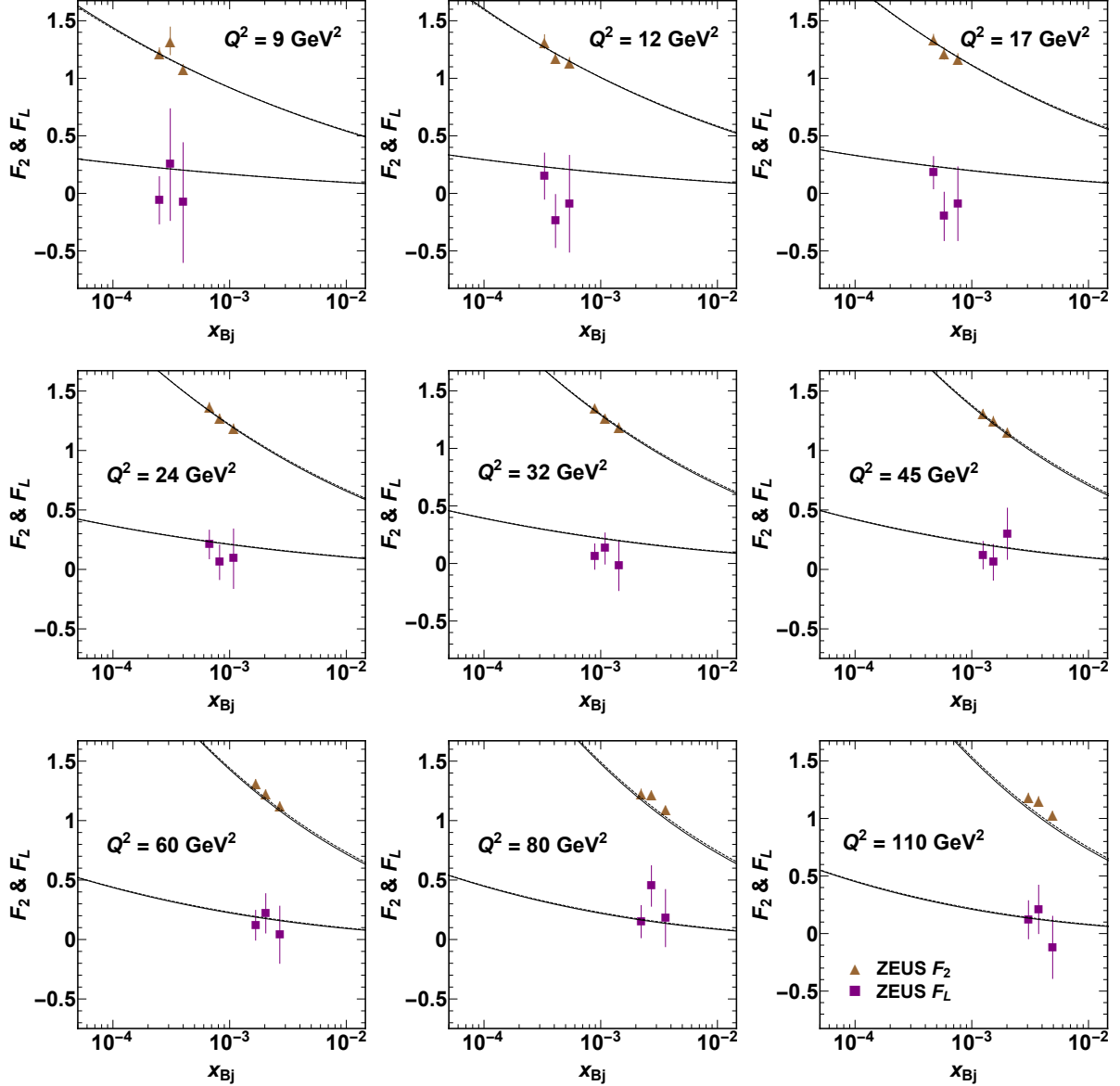


FIG. 7: Results for the longitudinal structure function $F_L(x, Q^2)$ and the structure function $F_2(x, Q^2)$, as functions of x , for different values of Q^2 . The solid and dashed lines are generated using parameter sets from table I, which correspond to charm masses of $m_c = 1.4 \text{ GeV}$ and $m_c = 1.27 \text{ GeV}$, respectively. The experimental data are from ZEUS collaboration [61].

as well as F_L and $F_2^{c\bar{c}}$, were not taken into account in the fitting process and hence they are predictions of the NLO dipole model. As can be observed in Figs. 3, 4, 5 and 7 it is clear that the NLO dipole model results exhibit strong agreement with the data on structure functions, over a wide kinematic range: for $Q^2 \in [0.85, 650] \text{ GeV}^2$. Evidently, the model demonstrates a solid consistency with the data, especially with regard to the structure functions F_2 and $F_2^{c\bar{c}}$ for which the experimental data are known for their higher precision. This consistency can also be taken as a non-trivial test of the model's accuracy, originating from the two critical parameters that determine high-energy scattering. This enables the theoretical results to be aligned with the available experimental data.

For the F_2 and $F_2^{c\bar{c}}$ we confronted our theoretical estimates with H1 + ZEUS combined data [48] while for F_L we have compared with the data from ZEUS collaboration [61]. As far as the structure functions F_2 is concerned, the agreement with the data remains valid for $x > 10^{-2}$ and only begins to weaken as we approach to $x \approx 10^{-1}$. Fig. 4 illustrates the $F_2^{c\bar{c}}$ data under the assumption that $\sigma_r^{c\bar{c}} \approx F_2^{c\bar{c}}$. It is important to note that the contribution of $F_L^{c\bar{c}}$ to the reduced cross-section (see Eq. (7)), arising from the exchange of longitudinally polarized photons, can be

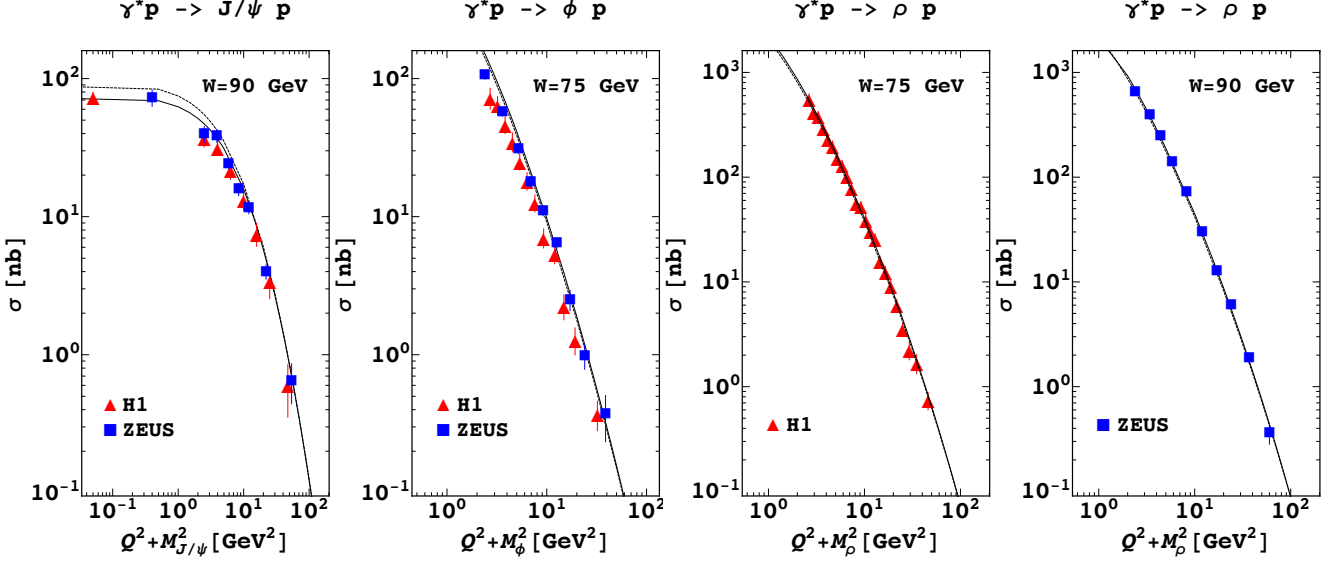


FIG. 8: Total vector meson cross-sections σ for J/ψ , ϕ and ρ , as a function of $Q^2 + M_V^2$ compared to theoretical estimates from CGC/saturation NLO dipole model where solid ($m_c = 1.4 \text{ GeV}$) and dashed ($m_c = 1.27 \text{ GeV}$) lines correspond to parameters of set I and set II, respectively. The data are from H1 and ZEUS collaborations [62–68].

approximately or even less than a few percent, making it negligible within the considered kinematic range. The data in Fig. 7 illustrates that the model results are characterized by a remarkable level of precision using the two parameter sets specified in Table I. Nevertheless, more accurate measurements of F_L data are required. In Figs. 3, 4 and 7 we extend our theoretical results outside the kinematics of existing data, as predictions for future DIS experiments.

Special comments deserve Fig. 5 and Fig. 6. In the former, we present the F_2 data as a function of Q^2 at various fixed x values. The characteristic features of this figure is that we are able to describe data for the range $x < 0.013$ with high accuracy, with both $m_c = 1.4 \text{ GeV}$ and $m_c = 1.27 \text{ GeV}$. Conversely, outside the fitting range, set II demonstrates effectiveness in reproducing data at the fixed $x = 0.013$ value, whereas set I displays little dispersion from $Q^2 > 20 \text{ GeV}^2$ at the same x value. The latter, demonstrates how our fits describe the experimental data on F_2 at low values of Q^2 . One can see that the agreement with the experimental data is good even at low Q^2 where we have no solid theoretical bases for wave functions and we still have sophisticated good description. This illustrate the possibility to use the wave function of the virtual photon in perturbative QCD at rather low values of Q^2 .

To expand the testing of the CGC/saturation NLO dipole model, we will now examine the exclusive diffractive processes at HERA. For the total cross-section, in Eq. (9) we performed the integral over $|t|$ up 1 GeV^2 . In Figs. 8 and 9 we confront the experimental data from H1 and ZEUS with our theoretical predictions for Q^2 and W -dependence of the vector mesons J/ψ , ϕ and ρ production in different kinematics. We present our model results computed using two parameter sets from table I, which correspond to charm mass values of $m_c = 1.4 \text{ GeV}$ and $m_c = 1.27 \text{ GeV}$. These results are represented by solid and dashed lines, respectively. One can see that the agreement is excellent, particularly in the case of vector meson J/ψ , the wave function (specified in Eqs. (15), (16), and (17)) is proficient at replicating experimental data, even at lower values of $Q^2 + M_{J/\psi}^2$ (see Fig. 8). Notice that both parameter sets give similar estimates, however for the case of vector meson J/ψ production, its total cross-section exhibits heightened sensitivity to the charm quark mass at low values of Q^2 (see Fig. 9) which differs from the behavior of lighter mesons ϕ and ρ . The reason for this lies in the fact that the scale in the integrand of the cross-section is established by ϵ_f as outlined in Eq. (5). It is only when virtualities are low, such as for $Q^2 < m_f^2$, that the cross-section starts to exhibit sensitivity to the quark mass.

In Fig. 10 we compared the NLO dipole model results for deeply virtual Compton scattering with the experimental data from H1 and ZEUS collaboration [68, 69]. In the left panel, we illustrate the Q^2 -dependence of the cross-section at fixed values of $W = 82 \text{ GeV}$ and $W = 104 \text{ GeV}$. This behavior remains consistent for both parameter sets provided in table I. Within the right panel, we present the W -dependence of the cross-section for different fixed Q^2 values. It

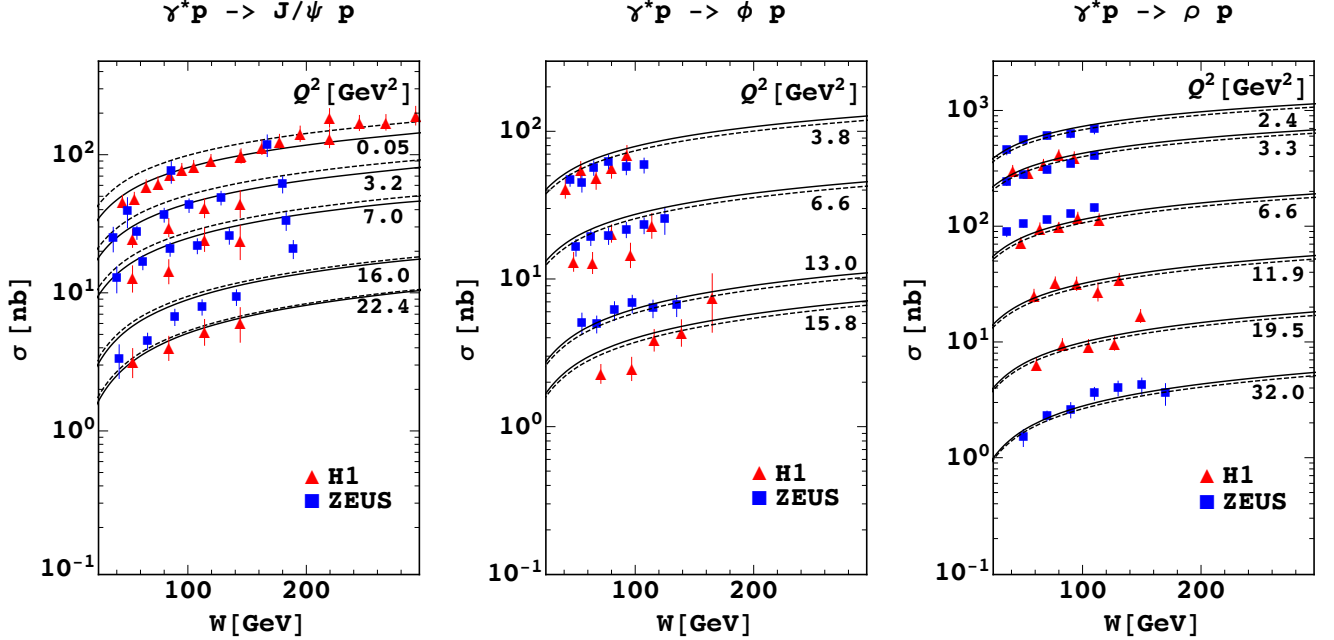


FIG. 9: Total vector meson cross-sections σ for J/ψ , ϕ and ρ , as a function of W . The solid lines correspond to parameters of set I ($m_c = 1.4$ GeV) and the dashed lines correspond to parameters of set II ($m_c = 1.27$ GeV). The data are from H1 and ZEUS collaborations [62–68].

demonstrates remarkable consistency with the experimental data. However, we cannot compare this specific model result with other saturation models since Refs. [31, 34, 44, 45] do not provide theoretical estimates for low photon virtuality. Nevertheless, a similar situation is encountered in Ref. [46] as in this paper’s discussion to lower Q^2 values (see figure 8-a from Ref. [46]). The total cross section for DVCS becomes more sensitive for low Q^2 . This is because the effects of the internal structure and the underlying dynamics of the proton, are more prominent.

In Figs. 11 and 12 we present the ratio of the longitudinal to the transverse cross-sections $R = \sigma_L/\sigma_T$ for J/ψ , ϕ and ρ vector meson production as a function of Q^2 and W , respectively. One can predict that the ratio $R = \sigma_L/\sigma_T$ will exhibit an increase as Q^2 grows. This is due to the fact that the ratio R conveys essential information about the effective average transverse size of the dipole involved in the interactions. Larger dipole sizes tend to predominantly influence the transverse component of the cross-section in contrast to the longitudinal component. Consequently, this results in a relative rise of the t -slope for the transverse component when compared to the longitudinal component. In Figure 11, our predictions were generated at a constant value of $W = 90$ GeV, while the plot displays the range of W -bins in the experimental data. Nonetheless, the W dependency of the ratio remains notably weak under the condition of a fixed Q^2 [62–67]. Fig. 12 show that σ_L and σ_T exhibit identical dependencies on W , which are determined by the gluon distribution [57]. Consequently, the ratio remains constant. The weak dependence of R on W observed in this paper is consistent with both the MRT [57] and FS04 models [70].

Finally, results for the slope B_D of t -distribution of exclusive vector meson electroproduction and DVCS is presented in Figs. 13 and 14. One can see that the agreement of the model with the experimental data is reasonable. The slope B_D values for lighter vector mesons, at the same Q^2 , are higher than those for J/ψ vector meson production, consistent with the experimental data. The reason for this lies in the convolution of the photon wavefunction with the vector meson wavefunction. It leads to different typical dipole sizes for light and heavy mesons, mainly determined by $1/\epsilon_f$ as described in equation Eq. (5). Hence, at a fixed virtuality, the typical dipole size is larger for lighter vector mesons, which, in turn, extends the range of validity for the asymptotic expression to higher Q^2 .

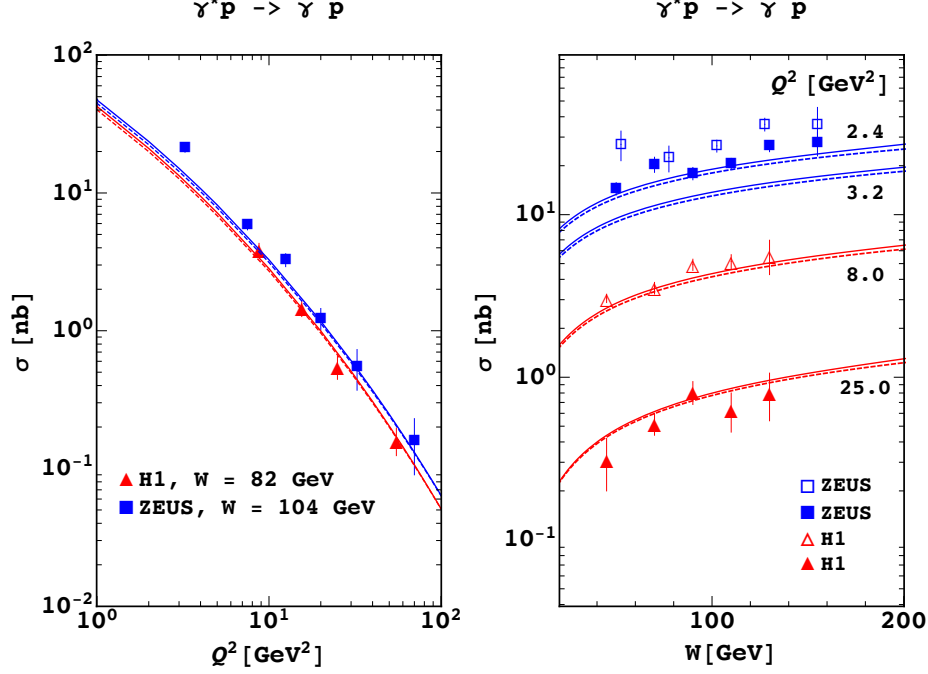


FIG. 10: Left: The Q^2 dependence of the cross section for DVCS. Right: The energy dependence of the cross section for DVCS. For theoretical results we use the parameters set given in table I $m_c = 1.4 \text{ GeV}$ in solid lines and $m_c = 1.27 \text{ GeV}$ in dashed lines. The data are from H1 and ZEUS collaborations [68, 69].

V. CONCLUSIONS

In this paper, we confronted the CGC/saturation NLO dipole model of Ref. [1] with the experimental combined HERA data, determining its parameters through the fitting procedure to the deep inelastic structure function F_2 and the reduced cross-section σ_r at small- x . Based on this approach, the re-summation procedure of Ref. [4–6] was included to fix the BFKL kernel in the NLO, albeit with an alternative treatment of the nonlinear corrections which leads to additional change of the NLO kernel of the evolution equation. The model incorporates the NLO corrections not only deep within the saturation domain but also in the proximity of the saturation scale, as well as two essential ingredients: *i*) the correct solution to the non-linear BK evolution equation in the saturation region, and *ii*) the impact parameter distribution that results in an exponential decrease of the saturation momentum as the impact parameter b becomes large and a power-like decrease at high momentum transfers, in accordance with the principles of perturbative QCD. Our approach differs from other attempts in that we propose $Q_s^2 \propto \exp(-mb)$ for large b , whereas in other models, Gaussian behavior at large b is assumed, with $Q_s^2 \propto \exp(-b^2/B)$. The exponential b dependence of Q_s^2 results in the exponential decrease of the scattering amplitude at large b , satisfying the Froissart theorem [21].

The model results are confronted to F_2 , $F_2^{c\bar{c}}$, F_L , as well as for exclusive diffractive processes such as vector meson production and DVCS with the available data from HERA. Using four fitting parameters we obtain good overall agreement with the experimental data in the range $Q^2 \in [0.85, 650] \text{ GeV}^2$ and $x < 10^{-2}$. The extracted CGC/saturation NLO dipole model give the saturation scale for proton $Q_s^2 < 1 \text{ GeV}^2$ in accord with other saturation models [44, 45]. It was illustrated that the CGC/saturation NLO dipole model provides an accurate representation of most aspects in both inclusive DIS and exclusive diffractive data, encompassing the Q^2 , W and x dependence. In Figs. 3, 4, 7, 9 and 10, we extend our theoretical estimates outside the kinematics of existing data, as predictions for forthcoming DIS experiments. The slope B_D of t -distribution of exclusive vector meson electroproduction, including J/ψ , ϕ , ρ as well as DVCS can be correctly reproduced, even though the wave functions of the vector mesons and DVCS are quite different. This provides a strong indication of the consistency in the core dynamics and emphasizes

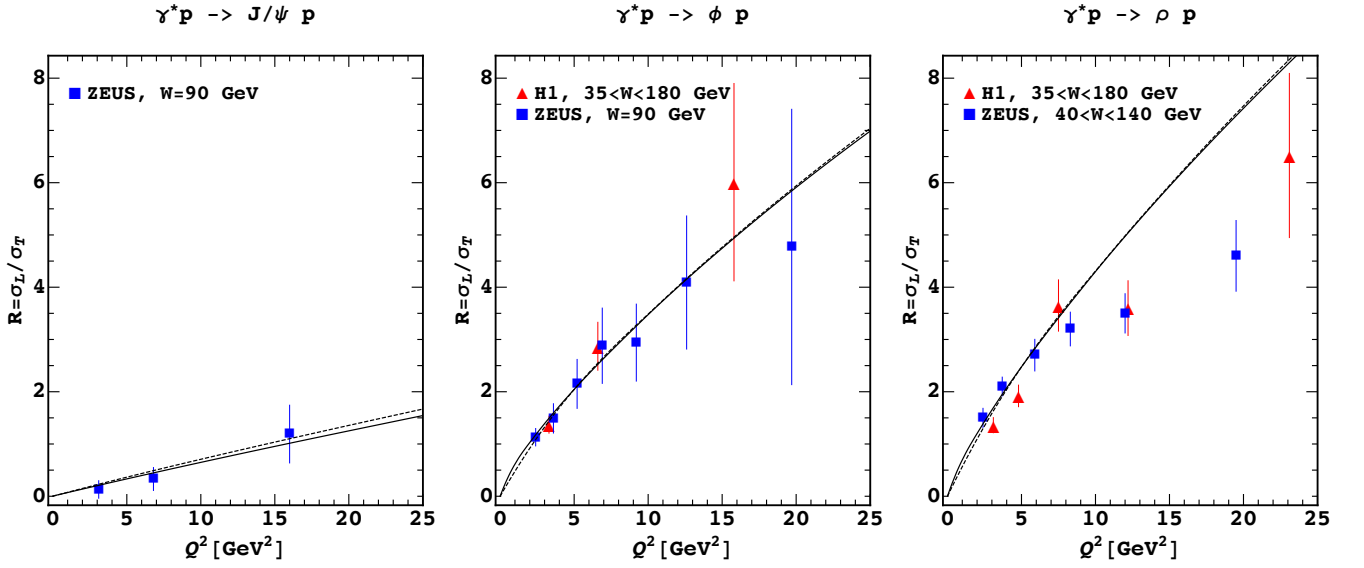


FIG. 11: The ratio $R = \sigma_L/\sigma_T$ for J/ψ , ϕ and ρ as a function of Q^2 . The solid ($m_c = 1.4$ GeV) and dashed ($m_c = 1.27$ GeV) lines correspond to parameter sets I and II, respectively. The experimental data are from H1 and ZEUS collaboration [62–67].

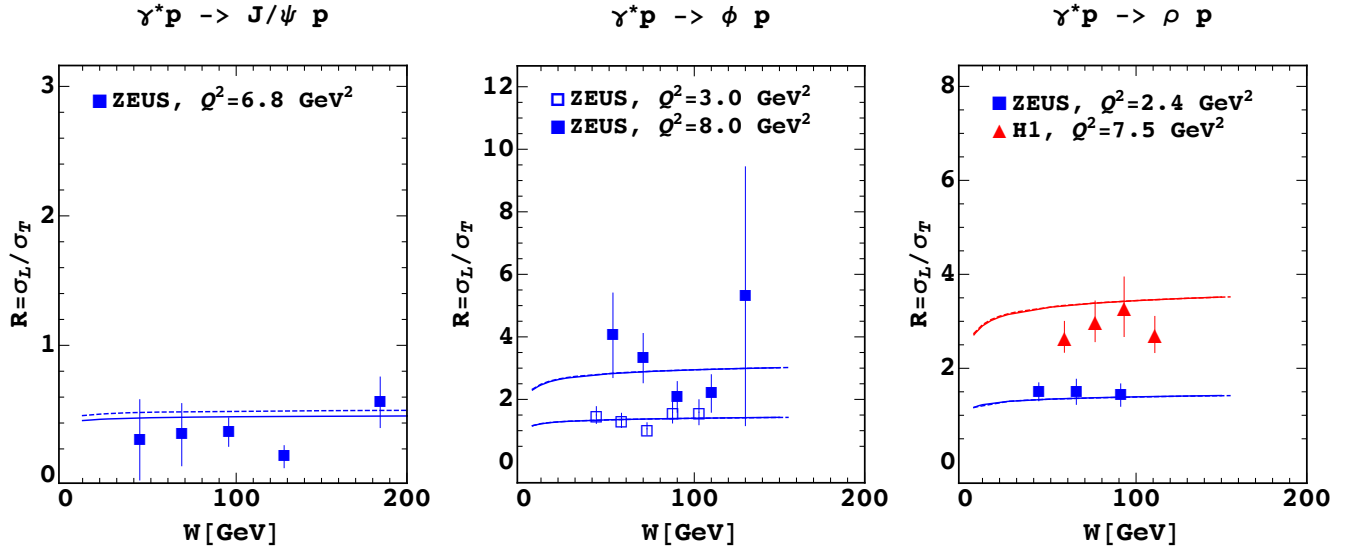


FIG. 12: The ratio $R = \sigma_L/\sigma_T$ for J/ψ , ϕ and ρ as a function of W . The solid and dashed lines are obtained using two distinct sets of parameters from table I corresponding to charm mass values of $m_c = 1.4, 1.27$ GeV, respectively. The experimental data are from H1 and ZEUS collaborations [62–67].

the crucial nature of the impact parameter dependence in the saturation scale within the proton. Additionally, our model successfully replicates the experimental data for the ratio $R = \sigma_L/\sigma_T$. This observation bolsters the idea that the transverse dimensions of the dipole play a key role in determining the appropriate length scale for interactions with both transverse and longitudinally polarized virtual photons.

Our results provide a strong guide for finding an approach, based on Color Glass Condensate/saturation effective theory for high energy QCD, to make reliable predictions from first principles, as well as for upcoming DIS experiments. We believe that the model presented here, will be a useful tool to estimate the CGC/saturation effects in a variety of reactions, including the production of dijets in p-p and p-Pb collisions or the structure of the soft Pomeron in CGC. The model takes into account all the theoretical understanding we have regarding deep inelastic processes and, thus, can be used for comparisons at high energy. In summary, we firmly believe that our model is the only path forward

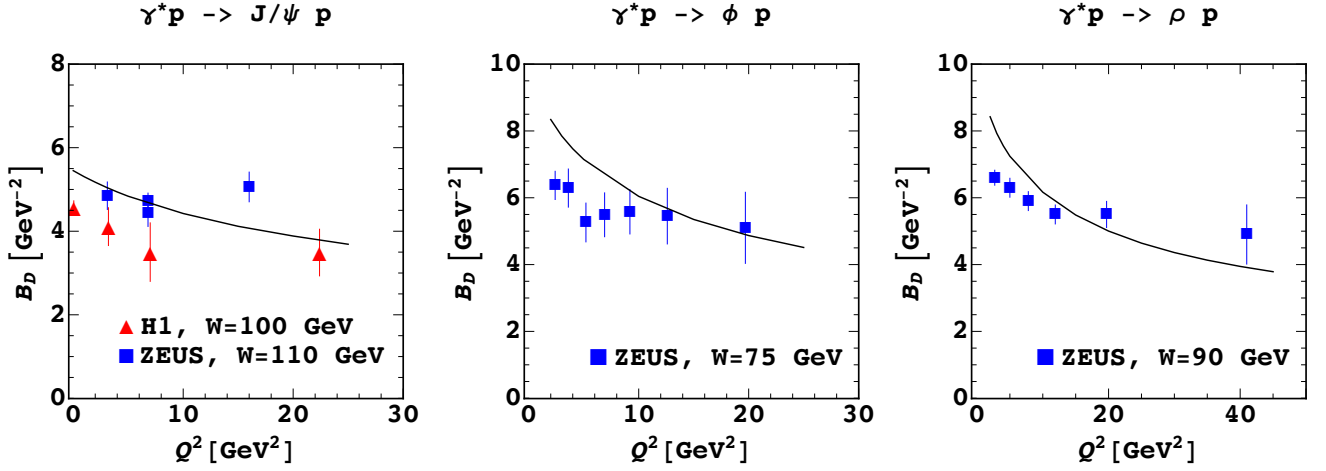


FIG. 13: Results for the slope B_D of t -distribution of exclusive vector meson electroproduction as a function of Q^2 employing the parameters from set I. The collection of experimental data are from H1 and ZEUS collaboration [62–67].

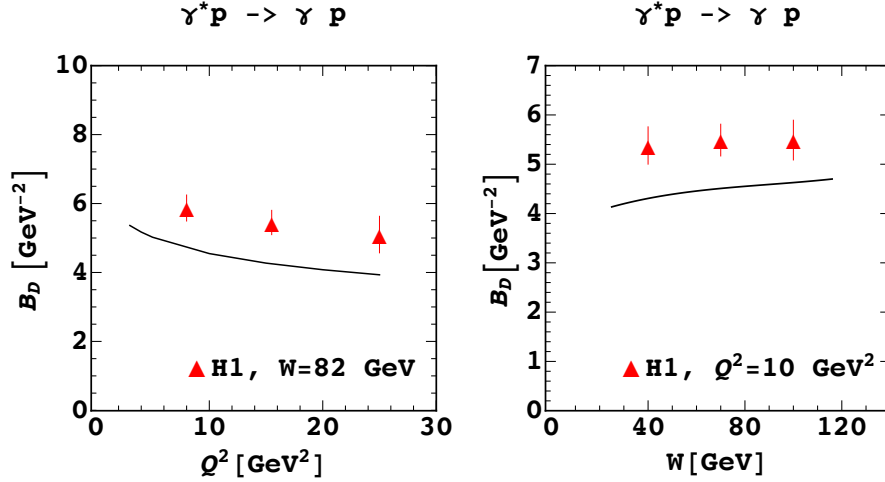


FIG. 14: Results for the slope B_D of t -distribution of DVCS processes as a function of Q^2 and W using parameters of set I. The collection of experimental data are from H1 and ZEUS collaboration [68, 69].

based on solid theoretical ground to extending predictions to higher energy, including those present at the LHC.

VI. ACKNOWLEDGEMENTS

We thank our colleagues at UPLA and UTFSM for encouraging discussions, and for the use of computing infrastructure of the Scientific and Technological Center of Valparaiso, Universidad Técnica Federico Santa María (ANID PIA/APOYO AFB180002). Our special thanks go to M. Siddikov for all his suggestion on this paper. This work was supported by Plan de Fortalecimiento de Universidades Estatales, UPA 19101, CR 18.180, Código 2390, Universidad de Playa Ancha and ANID Grant No 3230699 (MR), and Grant No 008/2023, DPP, Universidad Técnica Federico Santa María (JG).

* Electronic address: michael.roa@upla.cl

† Electronic address: jose.garridom@sansano.usm.cl

[‡] Electronic address: miguel.guevara@upla.cl

- [1] C. Contreras, E. Levin, R. Meneses and M. Sanhueza, “*Non-linear equation in the re-summed next-to-leading order of perturbative QCD: the leading twist approximation*,” Eur. Phys. J. C **80** (2020) no.11, 1029 [arXiv:2007.06214 [hep-ph]].
- [2] J. Jalilian-Marian, A. Kovner, A. Leonidov and H. Weigert, *Phys. Rev.* **D59**, 014014 (1999), [arXiv:hep-ph/9706377]; *Nucl. Phys.* **B504**, 415 (1997), [arXiv:hep-ph/9701284]; J. Jalilian-Marian, A. Kovner and H. Weigert, *Phys. Rev.* **D59**, 014015 (1999), [arXiv:hep-ph/9709432]; A. Kovner, J. G. Milhano and H. Weigert, *Phys. Rev.* **D62**, 114005 (2000), [arXiv:hep-ph/0004014]; E. Iancu, A. Leonidov and L. D. McLerran, *Phys. Lett.* **B510**, 133 (2001); [arXiv:hep-ph/0102009]; *Nucl. Phys.* **A692**, 583 (2001), [arXiv:hep-ph/0011241]; E. Ferreira, E. Iancu, A. Leonidov and L. McLerran, *Nucl. Phys.* **A703**, 489 (2002), [arXiv:hep-ph/0109115]; H. Weigert, *Nucl. Phys.* **A703**, 823 (2002), [arXiv:hep-ph/0004044].
- [3] I. Balitsky, [arXiv:hep-ph/9509348]; *Phys. Rev.* **D60**, 014020 (1999) [arXiv:hep-ph/9812311]; Y. V. Kovchegov, *Phys. Rev.* **D60**, 034008 (1999), [arXiv:hep-ph/9901281].
- [4] G. P. Salam, “*A Resummation of large subleading corrections at small x*,” *JHEP* **9807** (1998) 019 [hep-ph/9806482];
- [5] M. Ciafaloni, D. Colferai and G. P. Salam, “*Renormalization group improved small x equation*,” *Phys. Rev. D* **60** (1999) 114036 [hep-ph/9905566].
- [6] M. Ciafaloni, D. Colferai, G. P. Salam and A. M. Stasto, “*Renormalization group improved small x Green’s function*,” *Phys. Rev. D* **68** (2003) 114003, [hep-ph/0307188].
- [7] B. Ducloué, E. Iancu, A. H. Mueller, G. Soyez and D. N. Triantafyllopoulos, *JHEP* **04**, 081 (2019) [arXiv:1902.06637 [hep-ph]].
- [8] V. S. Fadin, E. A. Kuraev and L. N. Lipatov, “*On the pomeranchuk singularity in asymptotically free theories*”, *Phys. Lett.* **B60**, 50 (1975); E. A. Kuraev, L. N. Lipatov and V. S. Fadin, “*The Pomeranchuk Singularity in Nonabelian Gauge Theories*” *Sov. Phys. JETP* **45**, 199 (1977), [*Zh. Eksp. Teor. Fiz.*72,377(1977)]; I. I. Balitsky and L. N. Lipatov, “*The Pomeranchuk Singularity in Quantum Chromodynamics*,” *Sov. J. Nucl. Phys.* **28**, 822 (1978), [*Yad. Fiz.*28,1597(1978)].
- [9] L. N. Lipatov, “*Small x physics in perturbative QCD*,” *Phys. Rept.* **286**, 131 (1997) [hep-ph/9610276]; “*The Bare Pomeron in Quantum Chromodynamics*,” *Sov. Phys. JETP* **63**, 904 (1986) [*Zh. Eksp. Teor. Fiz.* **90**, 1536 (1986)].
- [10] E. Levin and K. Tuchin, “*Solution to the evolution equation for high parton density QCD*,” *Nucl. Phys.* **B573**, 833 (2000) [hep-ph/9908317]; “*New scaling at high-energy DIS*,” *Nucl. Phys.* **A691**, 779 (2001) [hep-ph/0012167]; “*Nonlinear evolution and saturation for heavy nuclei in DIS*,” **693**, 787 (2001) [hep-ph/0101275].
- [11] C. Contreras, E. Levin, R. Meneses and I. Potashnikova, “*CGC/saturation approach: a new impact-parameter dependent model in the next-to-leading order of perturbative QCD*,” *Phys. Rev. D* **94**, no.11, 114028 (2016) [arXiv:1607.00832 [hep-ph]].
- [12] W. Xiang, Y. Cai, M. Wang and D. Zhou, “*Rare fluctuations of the S-matrix at NLO in QCD*,” *Phys. Rev.* **D99** (2019) no.9, 096026 [arXiv:1812.10739 [hep-ph]].
- [13] I. Balitsky, “*Quark contribution to the small-x evolution of color dipole*,” *Phys. Rev. D* **75** (2007) 014001, [hep-ph/0609105].
- [14] Y. V. Kovchegov and H. Weigert, “*Triumvirate of Running Couplings in Small-x Evolution*,” *Nucl. Phys.* **A784** (2007) 188, [hep-ph/0609090].
- [15] I. Balitsky and G. A. Chirilli, “*Next-to-leading order evolution of color dipoles*”, *Phys. Rev.* **D77** (2008) 014019 [arXiv:0710.4330 [hep-ph]].
- [16] I. Balitsky and G. A. Chirilli, “*Rapidity evolution of Wilson lines at the next-to-leading order*”, *Phys. Rev.* **D88** (2013) 111501, [arXiv:1309.7644 [hep-ph]].
- [17] A. Kovner, M. Lublinsky, and Y. Mulian, “*Jalilian-Marian, Iancu, McLerran, Weigert, Leonidov, Kovner evolution at next to leading order*”, *Phys. Rev.* **D89** (2014) no. 6, 061704, [arXiv:1310.0378 [hep-ph]].
- [18] A. Kovner, M. Lublinsky, and Y. Mulian, “*NLO JIMWLK evolution unabridged*”, *JHEP* **08** (2014) 114, [arXiv:1405.0418 [hep-ph]].
- [19] M. Lublinsky and Y. Mulian, “*High Energy QCD at NLO: from light-cone wave function to JIMWLK evolution*”, *JHEP* **05** (2017) 097, [arXiv:1610.03453 [hep-ph]].
- [20] Yuri V Kovchegov and Eugene Levin, “*Quantum Chromodynamics at High Energies*”, Cambridge Monographs on Particle Physics, Nuclear Physics and Cosmology, Cambridge University Press, 2012 .
- [21] M. Froissart, *Phys. Rev.* **123** (1961) 1053;
A. Martin, “*Scattering Theory: Unitarity, Analyticity and Crossing*.” Lecture Notes in Physics, Springer-Verlag, Berlin-Heidelberg-New-York, 1969.
- [22] A. Kovner and U. A. Wiedemann, *Phys. Rev. D* **66**, 051502 (2002) [hep-ph/0112140]; *Phys. Rev. D* **66**, 034031 (2002) [hep-ph/0204277]; *Phys. Lett. B* **551**, 311 (2003) [hep-ph/0207335].
- [23] E. Ferreira, E. Iancu, K. Itakura and L. McLerran, “*Froissart bound from gluon saturation*,” *Nucl. Phys.* **A710**, 373 (2002) [hep-ph/0206241].
- [24] J. Bartels, E. Levin, *Nucl. Phys.* **B387** (1992) 617-637; L. McLerran, M. Praszalowicz, *Acta Phys. Polon.* **B42** (2011) 99, [arXiv:1011.3403 [hep-ph]] **B41** (2010) 1917-1926, [arXiv:1006.4293 [hep-ph]]; M. Praszalowicz, *Acta Phys. Polon. B* **42** (2011) 1557 [arXiv:1104.1777 [hep-ph]]; M. Praszalowicz and T. Stebel, *JHEP* **1303** (2013) 090 [arXiv:1211.5305 [hep-ph]]; L. McLerran, M. Praszalowicz and B. Schenke, *Nucl. Phys. A* **916** (2013) 210 [arXiv:1306.2350 [hep-ph]]; M. Praszalowicz, *Phys. Lett. B* **727** (2013) 461 [arXiv:1308.5911 [hep-ph]]; L. McLerran and M. Praszalowicz, *Phys. Lett. B* **741** (2015) 246 [arXiv:1407.6687 [hep-ph]].
- [25] A. M. Stasto, K. J. Golec-Biernat, J. Kwiecinski, “*Geometric scaling for the total gamma* p cross-section in the low x region*,” *Phys. Rev. Lett.* **86** (2001) 596-599, [hep-ph/0007192].
- [26] S. Bondarenko, M. Kozlov and E. Levin, “*QCD saturation in the semi-classical approach*,” *Nucl. Phys.* **A727** (2003), 139-178 [arXiv:hep-ph/0305150 [hep-ph]].
- [27] K. J. Golec-Biernat and M. Wusthoff, “*Saturation in diffractive deep inelastic scattering*,” *Phys. Rev.* **D60** (1999) 114023

- [hep-ph/9903358]; “Saturation effects in deep inelastic scattering at low Q^{*2} and its implications on diffraction,” Phys. Rev. **D59** (1998) 014017; [hep-ph/9807513].
- [28] J. Bartels, K. J. Golec-Biernat and H. Kowalski, “A modification of the saturation model: DGLAP evolution,” Phys. Rev. **D66** (2002) 014001 [hep-ph/0203258].
- [29] H. Kowalski and D. Teaney, “An Impact parameter dipole saturation model,” Phys. Rev. **D68** (2003) 114005 [hep-ph/0304189].
- [30] E. Iancu, K. Itakura and S. Munier, “Saturation and BFKL dynamics in the HERA data at small x ,” Phys. Lett. **B590** (2004) 199 [hep-ph/0310338].
- [31] H. Kowalski, L. Motyka and G. Watt, “Exclusive diffractive processes at HERA within the dipole picture,” Phys. Rev. **D74** (2006) 074016 [hep-ph/0606272].
- [32] H. Kowalski, T. Lappi and R. Venugopalan, “Nuclear enhancement of universal dynamics of high parton densities,” Phys. Rev. Lett. **100** (2008) 022303 [arXiv:0705.3047 [hep-ph]].
- [33] H. Kowalski, T. Lappi, C. Marquet and R. Venugopalan, “Nuclear enhancement and suppression of diffractive structure functions at high energies,” Phys. Rev. **C78** (2008) 045201 [arXiv:0805.4071 [hep-ph]].
- [34] G. Watt and H. Kowalski, “Impact parameter dependent colour glass condensate dipole model,” Phys. Rev. **D78** (2008) 014016 [arXiv:0712.2670 [hep-ph]].
- [35] E. Levin and A. H. Rezaeian, “Gluon saturation and inclusive hadron production at LHC,” Phys. Rev. **D82** (2010) 014022 [arXiv:1005.0631 [hep-ph]].
- [36] A. H. Rezaeian, “CGC predictions for $p+A$ collisions at the LHC and signature of QCD saturation,” Phys. Lett. **B718** (2013) 1058 [arXiv:1210.2385 [hep-ph]].
- [37] E. Levin and A. H. Rezaeian, “Gluon saturation and energy dependence of hadron multiplicity in pp and AA collisions at the LHC,” Phys. Rev. **D83** (2011) 114001 [arXiv:1102.2385 [hep-ph]].
- [38] E. Levin and A. H. Rezaeian, “Hadron multiplicity in pp and AA collisions at LHC from the Color Glass Condensate,” Phys. Rev. **D82** (2010) 054003 [arXiv:1007.2430 [hep-ph]].
- [39] D. Boer, M. Diehl, R. Milner, R. Venugopalan, W. Vogelsang, D. Kaplan, H. Montgomery and S. Vigdor *et al.*, “Gluons and the quark sea at high energies: Distributions, polarization, tomography,” [arXiv:1108.1713 [nucl-th]].
- [40] T. Lappi and H. Mantysaari, “Incoherent diffractive J/Ψ -production in high energy nuclear DIS,” Phys. Rev. **C83** (2011) 065202 [arXiv:1011.1988 [hep-ph]].
- [41] T. Toll and T. Ullrich, “Exclusive diffractive processes in electron-ion collisions,” Phys. Rev. **C87** (2013) 2, 024913 [arXiv:1211.3048 [hep-ph]].
- [42] P. Tribedy and R. Venugopalan, “Saturation models of HERA DIS data and inclusive hadron distributions in $p+p$ collisions at the LHC,” Nucl. Phys. A **850** (2011) 136 [Nucl. Phys. A **859** (2011) 185] [arXiv:1011.1895 [hep-ph]].
- [43] P. Tribedy and R. Venugopalan, “QCD saturation at the LHC: comparisons of models to $p+p$ and $A+A$ data and predictions for $p+Pb$ collisions,” Phys. Lett. **B710** (2012) 125 [Phys. Lett. **B718** (2013) 1154] [arXiv:1112.2445 [hep-ph]].
- [44] A. H. Rezaeian, M. Siddikov, M. Van de Klundert and R. Venugopalan, “IP-Sat: Impact-Parameter dependent Saturation model revised,” PoS DIS **2013** (2013) 060 [arXiv:1307.0165 [hep-ph]]; “Analysis of combined HERA data in the Impact-Parameter dependent Saturation model,” Phys. Rev. **D87** (2013) 3, 034002 [arXiv:1212.2974].
- [45] A. H. Rezaeian and I. Schmidt, “Impact-parameter dependent Color Glass Condensate dipole model and new combined HERA data,” Phys. Rev. **D88** (2013) 074016 [arXiv:1307.0825 [hep-ph]].
- [46] C. Contreras, E. Levin and I. Potashnikova, “CGC/saturation approach: a new impact-parameter dependent model,” Nucl. Phys. **A948** (2016), 1-18 [arXiv:1508.02544 [hep-ph]].
- [47] C. Contreras, E. Levin and M. Sanhueza, “Non-linear evolution in the re-summed next-to-leading order of perturbative QCD: confronting the experimental data,” [arXiv:2106.06214 [hep-ph]].
- [48] F. D. Aaron *et al.* [H1 and ZEUS Collaborations], “Combined Measurement and QCD Analysis of the Inclusive ep Scattering Cross Sections at HERA,” JHEP **1001** (2010) 109 [arXiv:0911.0884 [hep-ex]].
- [49] H. Abramowicz *et al.* [H1 and ZEUS Collaborations], “Combination and QCD Analysis of Charm Production Cross Section Measurements in Deep-Inelastic ep Scattering at HERA,” Eur. Phys. J. C **73** (2013) 2, 2311 [arXiv:1211.1182 [hep-ex]].
- [50] D. Boer, M. Diehl, R. Milner, R. Venugopalan, W. Vogelsang, D. Kaplan, H. Montgomery, S. Vigdor, A. Accardi and E. C. Aschenauer, *et al.* [arXiv:1108.1713 [nucl-th]]; R. Abdul Khalek, U. D’Alesio, M. Arratia, A. Bacchetta, M. Battaglieri, M. Begel, M. Boglione, R. Boughezal, R. Boussarie and G. Bozzi, *et al.* [arXiv:2203.13199 [hep-ph]].
- [51] J. L. Abelleira Fernandez *et al.* [LHeC Study Group], J. Phys. G **39** (2012), 075001 [arXiv:1206.2913 [physics.acc-ph]].
- [52] K. Kutak and S. Sapeta, Phys. Rev. D **86** (2012), 094043 [arXiv:1205.5035 [hep-ph]].
- [53] C. Contreras, E. Levin and M. Sanhueza, “Soft pomeron in the color glass condensate approach,” Phys. Rev. D **106** (2022) no.3, 034011 [arXiv:2203.10296 [hep-ph]].
- [54] J. Bartels, K. Golec-Biernat and K. Peters, Acta Phys. Polon. **B34**, 3051 (2003)
- [55] E. Gotsman, E. M. Levin and U. Maor, Z. Phys. C **57** (1993), 677-684 [arXiv:hep-ph/9209218 [hep-ph]].
- [56] J. Nemchik, N. N. Nikolaev and B. G. Zakharov, Phys. Lett. B **341** (1994), 228-237 [arXiv:hep-ph/9405355 [hep-ph]]; J. Nemchik, N. N. Nikolaev, E. Predazzi and B. G. Zakharov, Z. Phys. C **75** (1997), 71-87 [arXiv:hep-ph/9605231 [hep-ph]]; J. R. Forshaw, R. Sandapen and G. Shaw, Phys. Rev. D **69** (2004), 094013 [arXiv:hep-ph/0312172 [hep-ph]].
- [57] A. D. Martin, M. G. Ryskin and T. Teubner, Phys. Rev. D **62** (2000), 014022 [arXiv:hep-ph/9912551 [hep-ph]].
- [58] A. G. Shuvaev, K. J. Golec-Biernat, A. D. Martin and M. G. Ryskin, Phys. Rev. D **60** (1999), 014015 [arXiv:hep-ph/9902410 [hep-ph]].
- [59] E. Levin, “Dipole-dipole scattering in CGC/saturation approach at high energy: summing Pomeron loops,” JHEP **11** (2013), 039 [arXiv:1308.5052 [hep-ph]].

- [60] E. Iancu, K. Itakura and L. McLerran, “*Geometric scaling above the saturation scale,*” Nucl. Phys. **A708** (2002) 327 [hep-ph/0203137].
- [61] H. Abramowicz *et al.* [ZEUS Collaboration], “*Deep inelastic cross-section measurements at large y with the ZEUS detector at HERA,*” Phys. Rev. **D90** (2014) 7, 072002 [arXiv:1404.6376 [hep-ex]]; S. Chekanov *et al.* [ZEUS Collaboration], “*Measurement of the Longitudinal Proton Structure Function at HERA,*” Phys. Lett. **B682** (2009) 8 [arXiv:0904.1092 [hep-ex]].
- [62] S. Chekanov *et al.* [ZEUS], PMC Phys. A **1**, 6 (2007) [arXiv:0708.1478 [hep-ex]].
- [63] S. Chekanov *et al.* [ZEUS], Eur. Phys. J. C **24**, 345-360 (2002) [arXiv:hep-ex/0201043 [hep-ex]].
- [64] S. Chekanov *et al.* [ZEUS], Nucl. Phys. B **695**, 3-37 (2004) [arXiv:hep-ex/0404008 [hep-ex]].
- [65] A. Aktas *et al.* [H1], Eur. Phys. J. C **46**, 585-603 (2006) [arXiv:hep-ex/0510016 [hep-ex]].
- [66] S. Chekanov *et al.* [ZEUS], Nucl. Phys. B **718**, 3-31 (2005) [arXiv:hep-ex/0504010 [hep-ex]].
- [67] F. D. Aaron *et al.* [H1], JHEP **05**, 032 (2010) [arXiv:0910.5831 [hep-ex]].
- [68] S. Chekanov *et al.* [ZEUS], JHEP **05**, 108 (2009) [arXiv:0812.2517 [hep-ex]].
- [69] F. D. Aaron *et al.* [H1], Phys. Lett. B **681**, 391-399 (2009) [arXiv:0907.5289 [hep-ex]]; S. Chekanov *et al.* [ZEUS Collaboration], PMC Phys. **A1**, 6 (2007), [arXiv:0812.2517 [hep-ex]].
- [70] J. R. Forshaw and G. Shaw, JHEP **12** (2004), 052 [arXiv:hep-ph/0411337 [hep-ph]].